Adv. Polar Upper Atmos. Res., **14**, 66–75, 2000

Characteristics of solar flare effect in the high-latitude ionosphere as observed by the SuperDARN radars

Keisuke Hosokawa[1], Toshihiko Iyemori[2], Akira Sessai Yukimatu[3] and Natsuo Sato[3]

[1]*Department of Geophysics, Graduate School of Science, Kyoto University, Kitashirakawa-Oiwakecho, Sakyo-ku, Kyoto 606-8502*
[2]*Data Analysis Center for Geomagnetism Kyoto, Graduate School of Science, Kyoto University, Kitashirakawa-Oiwakecho, Sakyo-ku, Kyoto 606-8502*
[3]*National Institute of Polar Reserch, Kaga 1-chome, Itabashi-ku, Tokyo 173-8515*

Abstract: Sudden perturbations of the ground magnetic fields at solar flares are called geomagnetic Solar Flare Effect (SFE). An SFE is the extra ionization produced by the X-ray emission from a solar flare. We analyzed 10 intense SFE events from 1996 to 1998 using SuperDARN HF radar network and other instruments located in the northern hemisphere. Two typical ionospheric signatures associated with the solar flares are revealed, one is a sudden fade-out of backscatter echoes, and the other is an appearance or variation of field-aligned irregularities. Sudden fade-out is observed only in the sunlit hemisphere, and the appearance or variation of irregularities are observed only near the terminator. In addition, we investigated one event out of ten in detail and found that there exists a discontinuity of the electric field or conductivity around the irregularity. This fact suggests that the variation of conductivity or electric field in the *E* region could affect the irregularity formation in the *F* region.

1. Introduction

The sudden geomagnetic field variation following a solar flare is designated as a Solar Flare Effect (SFE). It is associated with the sudden change of ionospheric currents caused by the extra ionization produced by the X-ray and EUV radiation from the solar flare. Ohshio (1964) and Pinter (1967) pointed out that the region of enhanced conductivity responsible for SFE could be either the *D* region or the boundary between the *D* and *E* regions of the ionosphere. Solar flare emissions include impulsive and slow components, where the impulsive component is related to EUV radiation (90 to 1000 Å) and the slow component to soft X-ray (1 to 90 Å). The principal ionizing agent at the SFE is the soft X-ray. EUV emissions also cause an enhancement of plasma density in the *E* and *F* regions, but this effect is much smaller than that by X-rays (Donnelly, 1976). These SFE events are confined to the sunlit hemisphere, but Ohshio (1964), Sastri (1975) and Sastri and Murthy (1975) found the evidence of the possibility that SFE seems to occur even in the nightside hemisphere. Sudden fade-out of HF radio wave occurs simultaneously with the ionospheric SFE, which is due to an excess ionization in the ionosphere.

The SuperDARN radars observe the backscatter echo from the ionospheric

irregularities. These irregularities are due to the plasma density fluctuations which have been amplified through plasma instability processes (Fejer and Kelley, 1980; Keskinen and Ossakow, 1983; Tsunoda, 1988). Baker *et al.* (1986) have shown that the gradient-drift instability is responsible for the irregularity formation. The linear growth rate of field-aligned gradient-drift instabilities is proportional to the plasma velocity and inversely proportional to the plasma density gradient scale length. Then plasma density is one of the parameters controlling ionospheric irregularities. In this study, we investigated whether the plasma density and the electric field variations caused by SFE can affect the formation of irregularities or not. We have analyzed 10 intense SFE events which occurred during the period from 1996 to 1998 using the SuperDARN HF radar network in the northern hemisphere and other additional facilities, such as EISCAT, GOES satellite, IMAGE and Greenland magnetometer chains. In the first section, we explain the SuperDARN observation, and the second section is devoted to a case study of August 18, 1998 SFE event to explain the typical characteristics of SFE observed by the SuperDARN HF radars. In the last section, we summarize the general characteristics of the SFE events observed by the SuperDARN in the high-latitude ionosphere, and discuss the possible mechanisms.

2. SuperDARN

SuperDARN is an international collaborative project based on the network of coherent HF radars located in the high-latitude zones of the northern and southern hemispheres. The operation of the overall system is described by Greenwald *et al.* (1995). The northern component of the SuperDARN consists of six radars and their field of view covers the area from northern Scandinavia to northern Canada. In common time operations, the radars carry out azimuthal sweeps through discrete beam pointing directions numbered 0–15. The backscatter echoes are range-gated in steps of 45 km. Each 16-beam scan of the radar requires approximately 120 s. Thus, about 30 scans are carried out within each UT hour. The radar transmits on a selected frequency lying in 8–20 MHz, and detects the backscatter echo from the decameter-scale field-aligned irregularities in the ionospheric E and F region. Backscatter echoes from the region near the radar site (whose range is less than 800 km) come from the E region. Irregularities in the F region drift with the convective $\boldsymbol{E}\times\boldsymbol{B}$ motion (Ruohoniemi *et al.*, 1987). The Doppler shift in the backscattered signal provides us with the line-of-sight component of the $\boldsymbol{E}\times\boldsymbol{B}$ motion of plasmas.

3. A case study: August 18, 1998 event

A big flare (its X-ray flux observed by GOES is greater than $10^{-4}(W/m^2)$) occurred on August 18, 1998, and its associated geomagnetic SFE was observed at mid-latitudes and high-latitudes of the sunlit hemisphere. The onset of geomagnetic SFE was detected with GOES10 satellite X-ray flux, EISCAT electron density, IMAGE and Greenland ground magnetometers.

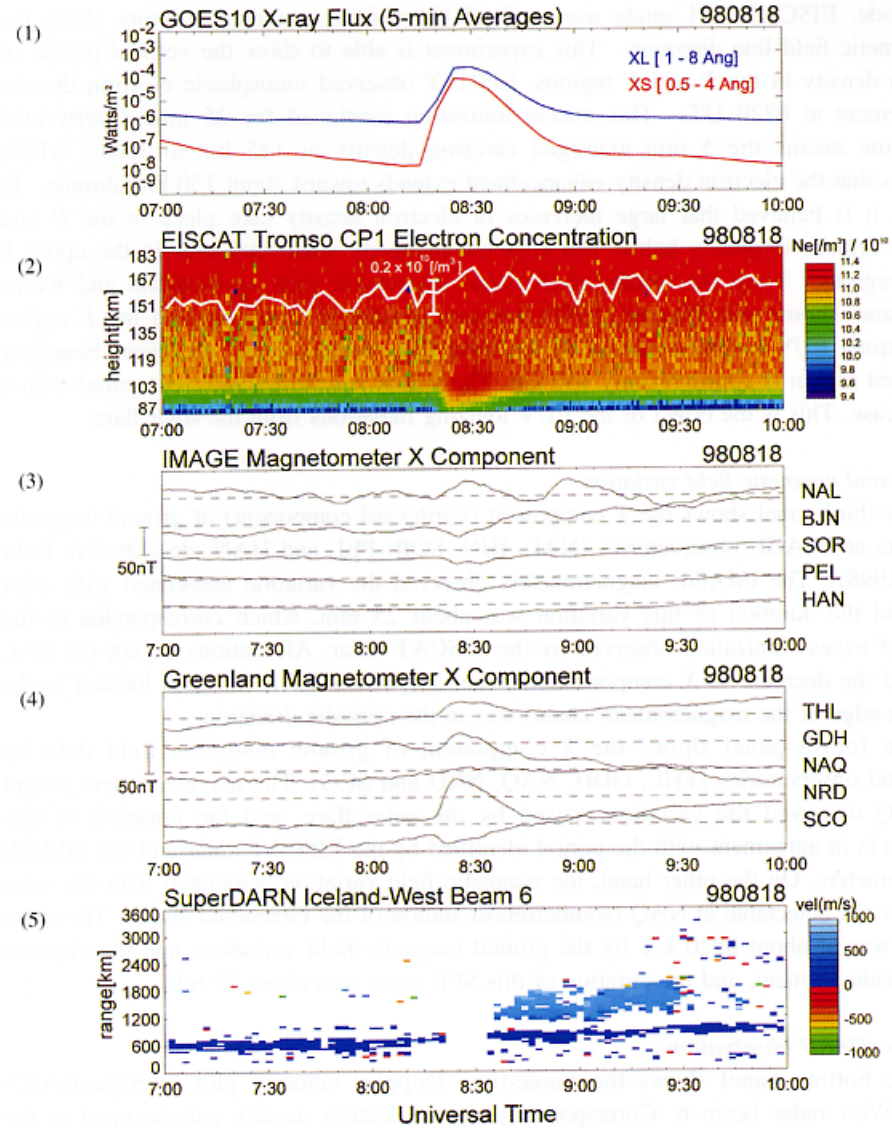

Fig. 2. Summary plot of GOES satellite X-ray flux, EISCAT electron density, IMAGE, Greenland ground magnetic field and Doppler velocity of SuperDARN Iceland-West radar beam6 for 3 hours from 0700 UT on August 18, 1998: (1) 5 min X-ray flux observed by GOES10; (2) EISCAT Tromsø CP1 mode electron density; (3) X component of IMAGE ground magnetic field (NAL, BJN, SOR, PEL, HAN); (4) X component of Greenland ground magnetic field (THL, GDH, NAQ, NRD, SCO); (5) line of sight Doppler velocity of SuperDARN Iceland-West radar beam6.

CP1 mode. EISCAT CP1 mode uses a fixed transmitting antenna, pointing along the geomagnetic field line direction. This experiment is able to show the vertical profile of electron density in the E and F regions. EISCAT observed ionospheric electron density enhancement at 0820 UT. This excess ionization continued for 25 min. Overwritten white line means the 5 min averaged electron density at 145 km altitudes, which indicates that the electron density enhancement extends toward about 150 km altitude. In general, it is believed that large increases of electron density take place in the D and lower E regions (typically below 100 km), but relatively small increases in the upper E and F regions. From the results of IS radar observation such as Mendillo and Evans (1974) and Thome and Wagner (1971), electron density was enhanced in the F region under strong EUV radiation caused by the solar flare. In this event, the upper boundary of ionized region is approximately 150 km. The height is a little higher compared with a typical case. This is the effect of the EUV ionizing radiations from the solar flare.

3.4. Ground magnetic field variation

The third panel shows the X component (northward component) of ground magnetic field data at IMAGE observatories (NAL, BJN, SOR, PEL and HAN, described in Lühr *et al.* (1998)). The IMAGE magnetometers observed the variation associated with solar flare, and the duration of this variation was about 25 min, which corresponded to the period of excess ionization observed by the EISCAT radar. All stations except for NAL observed the decrease in X component, but the variation at NAL (NAL is located in the northern edge of the magnetometer chain) was in the opposite direction.

The fourth panel shows the X component of ground magnetic field data by Greenland observatories (THL, GDH, NAQ, NRD and SCO). The magnetometers except for NAQ observed the variation caused by the solar flare, and the duration of this variation is in agreement with the period identified by the EISCAT radar and the IMAGE magnetometers. On the other hand, the magnetic field variation associated with the solar flare was not detectable at NAQ (southernmost station of the Greenland chain). The onset of SFE was at about 0820 UT by the ground magnetic field variations and the electron density enhancement, and the duration of this SFE event was about 25 min.

3.5. SuperDARN observation

The bottom panel shows the range-time Doppler velocity plot of SuperDARN Iceland-West radar beam 6. Corresponding to the electron density enhancement at the lower ionosphere, sudden fade-out of backscatter echo occurred and continued for 12 min. After the fade-out, an irregularity region appeared in the range of the F region. This irregularity region remained until 0930 UT.

Figure 3a shows the two dimensional line-of-sight Doppler velocity data obtained by the Iceland-East and West radars before and after the SFE, in geomagnetic coordinate system described in Baker and Wing (1989). The first panel shows the data at 20 min before the SFE onset (0800:00–0802:00 UT). At this time both radars received the echo only from the region whose range is below 800 km, and these echoes are considered to come from the E region. The second panel shows the snapshot during fade-out of radar echoes (0822:00–0824:00 UT). At this time, no echo was observed by both radars. This is probably because the radio absorption occurred at the D region and lower E region in

3.1. Location of the instruments

The configuration of all the observational instruments at the onset of SFE (0820 UT) is shown in Fig. 1. The field of view of EISCAT Tromsö CP1 mode is represented by an open circle in the auroral zone (geographical latitude of 68°–70°) of prenoon local time sector (about 1000 geographic local time) and the location of IMAGE and Greenland magnetometers are displayed by small circles. The SuperDARN Iceland-West radar and Iceland-East radar were in 0700 geographic local time sector. The field of view of Iceland-West radar covered the dawn-side region near the terminator (at 100 km altitude), and Iceland-East radar observed the dayside region. Greenland magnetometers were under the field of view of Iceland-West radar.

3.2. X-ray flux

Solar X-ray flux detected by GOES10 satellite, ionospheric electron density observed by EISCAT Tromsø CP1 mode, ground magnetic fields of IMAGE and Greenland chain and line of sight Doppler velocity of SuperDARN Iceland-West radar beam 6 are summarized in Fig. 2. The top panel shows the solar X-ray flux data observed by GOES10. The X-ray flux started to increase at 0815 UT and reached its maximum at 0825 UT. This X-ray flux enhancement continued until 0900 UT.

3.3. EISCAT observation

The second panel shows the electron density observed by EISCAT Tromsø radar

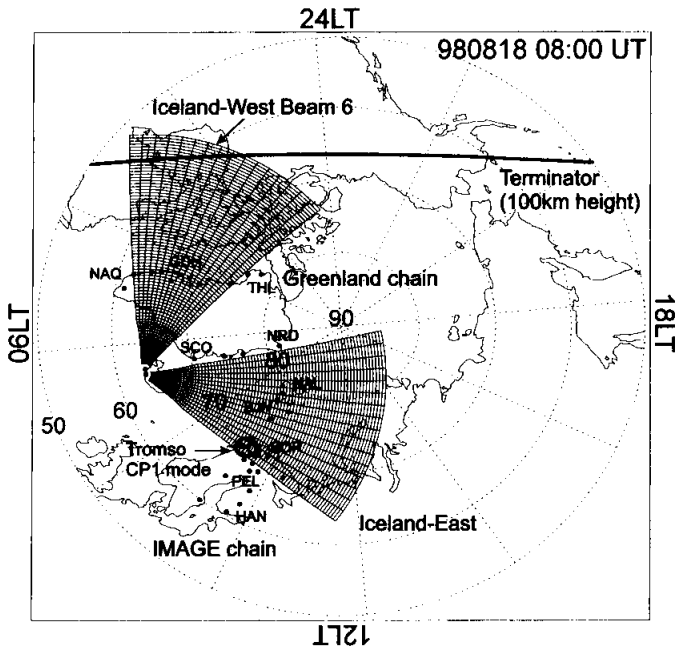

Fig. 1. The location of EISCAT Tromsö CP1 mode, IMAGE and Greenland magnetometer chains and SuperDARN Iceland-East and West in geographic coordinate at the onset of August 18, 1998 SFE event.

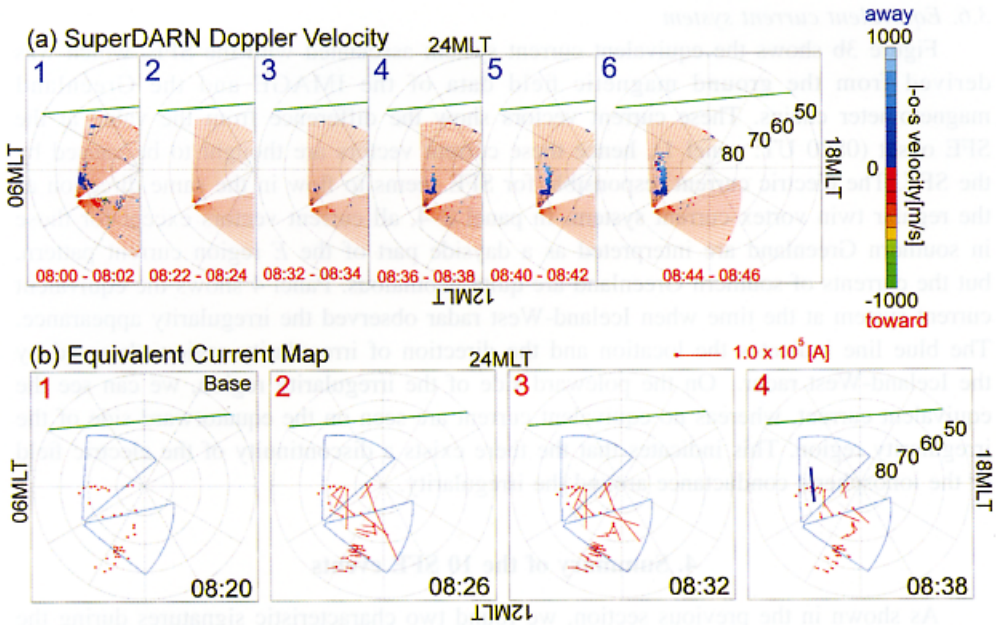

Fig. 3. (a) Two dimensional line of sight Doppler velocity map of August 18, 1998 SFE event in geomagnetic coordinate; (b) Equivalent current system associated with the SFE, which was deduced from the ground magnetic field data of the IMAGE and the Greenland magnetometer chains.

the field of view of the radar. The third panel shows the data immediately after the fade-out (0832:00–0834:00 UT). As seen in panel 3–panel 6, an irregularity appeared and expanded toward the terminator after the fade-out. Irregularities had a narrow band structure along the magnetic longitudinal direction. The line-of-sight Doppler velocity in this irregularity region is sunward, and the line-of-sight velocity at places distant from the radar site is higher than that near the radar.

The IMF observed by WIND was always southward ($Bz \approx -4$ nT) during the period from 0500 UT to 1000 UT, and no sudden variation such as southward turning was recorded before and after the SFE. These observed line-of-sight Doppler velocities are consistent with the *F* region convection model of Ruohoniemi and Greenwald (1996) in IMF *Bz* southward case. The *F* region convection model of Ruohoniemi and Greenwald (1996) was derived from the statistical study of the Doppler velocity data observed by SuperDARN Goose Bay radar. In addition, the elevation angle of backscatter from these irregularity region observed by the interferometer was ranged from 30° to 40° and the transmitting frequency was approximately 13 MHz. Villain *et al.* (1984) calculated the ray-path of 12.4 MHz HF wave for several elevation angles. Their results show that the HF wave with elevation angle less than 10° propagate to the *E* region height and cannot reach the *F* region. Therefore the propagation theory suggests that these echoes observed by Iceland-West came from *F* region irregularities. On the other hand, Iceland-East radar did not observe the irregularity in the dayside region.

3.6. Equivalent current system

Figure 3b shows the equivalent current system associated with the SFE, which was derived from the ground magnetic field data of the IMAGE and the Greenland magnetometer chains. These current vectors show the difference from the value at the SFE onset (0820 UT: panel 1), hence these current vectors are thought to be caused by the SFE. The electric current responsible for SFE seems to flow in the same direction as the regular twin vortex current system. In panel 2–4, all current vectors except for those in southern Greenland are interpreted as a dayside part of the *E* region current pattern, but the currents of southern Greenland are quite anomalous. Panel 4 shows the equivalent current system at the time when Iceland-West radar observed the irregularity appearance. The blue line indicates the location and the direction of irregularity region observed by the Iceland-West radar. On the poleward side of the irregularity region, we can see the equivalent current, whereas no equivalent current are seen on the equatorward side of the irregularity region. This indicates that the there exists a discontinuity of the electric field or the ionospheric conductance around the irregularity.

4. Summary of the 10 SFE events

As shown in the previous section, we found two characteristic signatures during the period of SFE, one is the radio fade-out and the other is the appearance or variation of ionospheric irregularity regions. Table 1 indicates the location of the radars for the 10 events when they observed these two signatures. The fields of view of radars are sorted by the local time, whether they are located on the dayside, near the terminator or on the nightside. The alphabet letters in Table 1 represent each radar (e: Iceland-East, f: Finland, w: Iceland-West, g: Goose Bay, k: Kapuskasing, t: Saskatoon). The circumflex letters mean that the radar observed sudden fade-out of echoes simultaneous with the SFE onset, and the capital letter alphabets mean that the radars observed appearance or variation of irregularity after the SFE. Sudden fade-out occurs only in the sunlit hemisphere and never in the dark hemisphere. This means that sudden fade-out of echo is due to the radio absorption caused by excess ionization in the *D* and *E* regions of the ionosphere. Another characteristic is that the irregularity associated with SFE appears or varies only near the terminator between 70° and 90° solar zenith angle at the ground level.

5. Discussion

At the onset of geomagnetic SFE, radio fade-out occurs at the SuperDARN radars located in the sunlit hemisphere, but it does not in the dark hemisphere. This indicates that a sudden fade-out is caused by the absorption of radio wave due to the extra ionization in the *D* and *E* region of the ionosphere.

In 5 of the 10 events, SuperDARN observed the appearance or variation of decameter-scale ionospheric irregularities after the onset of SFE. These irregularities are observed only by the radar whose field of view covers the region near the terminator. Here, the term "near the terminator" means the region with the solar zenith angle at ground level ranging between 70° to 90°. Previous work Baker *et al.* (1986) has shown

Table 1. The location of the radars when they observed fade-out and appearance or variation of irregularity region. The location of radars are sorted by the local time, whether they were on the dayside, near the terminator or on the nightside.

Date		Dayside	Terminator	Nightside
960709	0901 UT	ê f̂	ŵ	
971104	0552 UT			e f w g k t
971106	1149 UT		ê Ŵ F̂	g k t
971127	1259 UT			e f w g k t
980423	0535 UT		e f̂	w g k t
980502	1331 UT	ê f̂ ŵ ĝ k̂ t̂		
980817	2110 UT	k̂ ŵ	E F	
980818	0815 UT	ê f̂	Ŵ	k
980818	2210 UT	k̂	Ŵ	e f
980819	2135 UT	k̂	Ŵ	e f

Alphabet letters represent each radar (e: Iceland-East, f: Finland, w: Iceland-West, g: Goose Bay, k: Kapuskasing, t: Saskatoon), and the circumflex letters mean that the radar observed sudden fade-out simultaneous with SFE onset, and the capital letter alphabet means that the radar observed the appearance or variation of irregularity after SFE.

that the gradient-drift instability is responsible for some of the coherent scatter observed by the Goose Bay radar. The linear growth rate of field-aligned gradient-drift instabilities is proportional to the plasma velocity and inversely proportional to the plasma density gradient scale length. At the dawn and dusk meridians, and at the equatorward edge of the convection cell, photoionization produces a sunward directed plasma density gradient, and the level of the gradient is maximized near the terminator. The dominant plasma convection on that region is typically in the sunward direction, and electric field directs equatorward (Ruohoniemi and Greenwald, 1996; Weimer, 1995). In the event on August 18, 1998, the equatorward electric field estimated from Doppler velocity of Iceland-West radar is about 20–40 (mV/m) on the irregularity region. Thus the plasma density gradient and electric field produces the background conditions favorable to gradient-drift instabilities in dawn and dusk regions near the terminator.

The analysis of the equivalent current system in that event indicates the possibility that the gap of conductivity existed in the direction across the narrow band structure of irregularity. If the difference of the amount of current flow causes a charge accumulation at the boundary, an equatorward polarization electric field could appear. In addition, the resultant irregularity growth is opposed principally by cross-field ion diffusion, which is strongly influenced by the *E* region conductivity. From these facts, it could be argued that the sudden variation of ion diffusion rate or electric field in the *E* region caused by X-ray emission contributes to the *F* region irregularity formation as a trigger of instability process.

6. Summary

We investigated 10 intense solar flare events (their X-ray flux observed by GOES is greater than 10^{-4}(W/m^2)) during 1996–1998 using SuperDARN, EISCAT, GOES, IMAGE and Greenland ground magnetometer chains. All of these events are accompanied by the geomagnetic field variation known as the geomagnetic Solar Flare Effect.

We have clarified the two typical ionospheric signatures associated with the solar flares, one is a sudden fade-out of HF radio wave and the other is an appearance or variation of field aligned irregularities. Sudden fade-out is detected by the radars located in the sunlit hemisphere only, and the appearance or variation of irregularities are observed only near the terminator. We investigated one event in detail and found that there exists a discontinuity of the electric field or conductivity around the irregularity. This result suggests the possibility that the variation of conductance or electric field in the *E* region would affect the irregularity formation in the *F* region.

How the conductivity or the electric field in the *E* region contributes to the formation of irregularities in the *F* region during SFEs is still unknown. Detailed study using electron density and electric field data obtained by the IS radars in the irregularities and conductivity profile deduced from the ground magnetic field are needed to know which factor is most significant for the formation of irregularity during SFEs.

Acknowledgments

We are grateful to the PIs who operate the Iceland-West and Iceland-East radars. We thank the institutes who maintain the IMAGE magnetometer array. The IMAGE magnetometer data are collected as a Finnish-German-Norwegian-Polish-Russian-Swedish project, and the PI of IMAGE belongs to the Finnish Meteorological Institute. The data of Greenland magnetometer chain are managed by Danish Meteorological Institute (DMI), and we appreciate them for providing us with their data. We are indebted to the Director and staff of EISCAT for operating the facility and supplying the data. EISCAT is an International Association supported by Finland (SA), France (CNRS), the Federal Republic of Germany (MPG), Japan (NIPR), Norway (NFR), Sweden (NFR) and the United Kingdom (PPARC). This study has been supported in part by "Ground Research for Space Utilization" promoted by NASDA and Japan Space Forum and also by grant 10640430 under the Ministry of Education, Japan.

The editor thanks Drs. Tadahiko Ogawa and A. Rodger for their help in evaluating this paper.

References

Baker, K.B., Greenwald, R.A., Walker, A.D.M., Bythrow, P.F., Zanetti, L.J., Potemra, T.A., Hardy, D.A., Rich, F.J. and Rino, C.L. (1986): A case study of plasma processes in the dayside cleft. J. Geophys. Res., **91**, 3130–3144.

Baker, K.B. and Wing, S. (1989): A new magnetic coordinate system for conjugate studies at high latitudes. J. Geophys. Res., **94**, 9139–9143.

Donnelly, R.F. (1976): Empirical models of solar flare X ray and EUV emissions for use in studying their *E* and *F* region effects. J. Geophys. Res., **81**, 4745–4753.

Fejer, B.G. and Kelley, M.C. (1980): Ionospheric irregularities. Rev. Geophys., **18**, 401–454.

Greenwald, R.A., Baker, K.B., Dudeney, J.R., Pinnock, M., Jones, T.B., Thomas, E.C., Villain, J.-P., Cerisier, J.C., Senior, C., Hanuise, C., Hunsucker, R.D., Sofko, G., Koehlers, J., Nielsen, E., Pellinen, R., Walker, A.D.M., Sato, N. and Yamagishi, H. (1995): DARN/SuperDARN: A global view of high-latitude convection. Space Sci. Rev., **71**, 763–796.

Keskinen, M.J. and Ossakow, S.L. (1983): Theories of high-latitude ionospheric irregularities: A review. Radio Sci., **18**, 1077–1091.

Lühr, H., Aylward, A., Buchert, S.C., Pajunp, A., Pajunp, K., Holmboe, T. and Zalewski, S.M. (1998): Westward moving dynamic substorm features observed with the IMAGE magnetometer network and other ground-based instruments. Ann. Geophys., **16**, 425–440.

Mendillo, M. and Evans, J.V. (1974): Incoherent scatter observations of the ionospheric response to a large solar flare. Radio Sci., **9**, 197–203.

Ohshio, M. (1964): Solar flare effect on geomagnetic variation. J. Radio Res. Lab. Jpn., **11-58**, 377–491.

Pinter, S. (1967): Geomagnetic crochets of solar flares observed in Hurbanovo. Bull. Astron. Inst. Czech., **8**, 274–281.

Ruohoniemi, J.M., Greenwald, R.A., Baker, K.B., Villain, J.-P. and McCready, M.A. (1987): Drift motions of small-scale irregularities in the high-latitude *F* region: An Experimental comparison with plasma drift motions. J. Geophys. Res., **92**, 4553–4564.

Ruohoniemi, J.M. and Greenwald, R.A. (1996): Statistical patterns of high-latitude convection obtained from Goose Bay HF radar observations. J. Geophys. Res., **101**, 21743–21763.

Sastri, J.H. (1975): Night time geomagnetic effects of solar flares. Ann. Geophys., **31**, 389–343.

Sastri, J.H. and Murthy, B.S. (1975): Geomagnetic effects in the dark hemisphere associated with solar flares. J. Geomagn. Geoelectr., **27**, 67–73.

Thome, G.D. and Wagner, L.S. (1971): Electron density enhancements in the *E* and *F* regions of the ionosphere during solar flares. J. Geophys. Res., **76**, 6883–6895.

Tsunoda, R.T. (1988): High-latitude *F* region irregularities: A review and synthesis. Rev. Geophys., **26**, 719–760.

Villain, J.-P., Greenwald R.A. and Vickrey, J.F. (1984): HF ray tracing at high latitudes using measured meridional electron density distributions. Radio Sci., **19**, 359–374.

Weimer, D.R. (1995): Models of high-latitude electric potentials derived with a least error fit of spherical harmonic coefficients. J. Geophys. Res., **100**, 19595–19607.

(Received October 28, 1999; Revised manuscript accepted February 15, 2000)